An ESD Immunity Test for Battery-Operated Control Circuit Board in Myoelectric Artificial Hand System

Cheng JI[†], *Nonmember*, Daisuke ANZAI[†], *Member*, Jianqing WANG[†a)], *Fellow*, Ikuko MORI[††], *Member*, and Osamu FUJIWARA[†], *Fellow*

SUMMARY   We conduct, in accordance with IEC 61000-4-2, an electrostatic discharge (ESD) test for a small size battery-operated control circuit board in a myoelectric artificial hand system to investigate the influence of the induced noises by indirect ESDs from an ESD generator to a horizontal coupling plane (HCP) and a vertical coupling plane (VCP). A photo-coupler is set between the small size control board and a motor control circuit to suppress noise in the pulse width modulation (PWM) signals. Two types of ESD noise are observed at the output pins of PWM signals. One type is the ESD noise itself (called Type A) and the other one is the ESD noise superimposed over the PWM pulses (Type B). No matter which polarity the charge voltages of the ESD generator have, both types can be observed and the Type A is dominant in the output pulses. Moreover, the ESD interference in the HCP case is found to be stronger than that in the VCP case usually. In the PWM signals observed at the photo-coupler output, on the other hand, Type A noises tend to increase for positive polarity and decrease for negative polarity, while Type B noises tend to increase at $-8\,\mathrm{kV}$ test level in the HCP case. These results suggest that the photo-coupler does not work well for ESD noise suppression. One of the reasons has been demonstrated to be due to the driving capability of the photo-coupler, and other one is due to the presence of a parasitic capacitance between the input and output of the photo-coupler. The parasitic capacitance can yield a capacitive coupling so that high-frequency ESD noises pass through the photo-coupler.

key words: ESD, immunity test, control board, PWM signal, photo-coupler

1. Introduction

Electrostatic discharge (ESD) often occurs between two electrically charged objects and the induced ESD noise may range beyond GHz bands in frequency spectra. Such a noise may damage or upset the function of sensitive electronic circuits. From this perspective, the IEC 61000-4-2 standard [1], [2] is issued by the International Electrotechnical Commission (IEC) and regulates the ESD immunity test, in which an ESD generator or ESD gun is used for simulating the discharge from a charged human body to electronic devices.

The immunity test with an ESD gun can be divided into contact discharge and air discharge according to the difference between the methods used to inject the discharge current into the equipment under test (EUT). According to the target into which the output current from the ESD gun is injected, the immunity test can also be divided into direct test and indirect test. The direct test uses the ESD gun to discharge directly to the surface or a specific point of EUT and it simulates the situation of discharges from a charged human body to an electronic device. On the other hand, the indirect test can simulate the case when the human body touches a metallic object near electronic devices and it also uses the ESD gun to discharge to a metal plane placed close to EUT. In actual tests, these indirect discharges are simulated by a vertical coupling plane (VCP) and a horizontal coupling plane (HCP), respectively.

As regards the direct ESD immunity tests, some valuable results have been reported so far in [3]–[7] from the viewpoints of the correlation between EUT failure and ESD gun parameters, the reproducibility, uncertainty, as well as the prediction of discharge current waveforms from the ESD gun. For the indirect ESD immunity tests [8]–[10], there are few published investigations [11] for real EUT, although most manufacturers have been conducting all kinds of ESD immunity tests.

In this study, we conduct a case study on an indirect ESD immunity test for a small size battery-operated control board in a myoelectric artificial system in conformity with IEC 61000-4-2. Figure 1 shows the block diagram of a myoelectric artificial hand system. In this system, the myogenic potential signals in the order of mV are acquired by
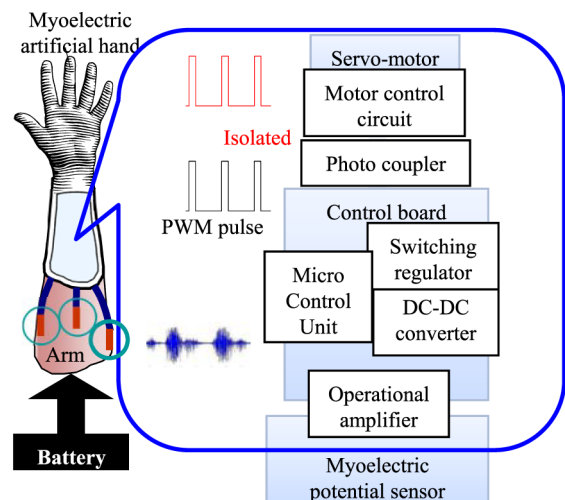
Fig. 1   Block diagram of myoelectric artificial hand system.

several sensors attached on the arm, and then are amplified and sent to a small size control board. The micro control unit in the control board analyzes the myogenic potential signals and produces the corresponding pulse width modulation (PWM) signals. The PWM signals are sent to a motor control unit at the hand for driving the servo-motors to make the artificial hand work. In order to suppress electromagnetic noises between the control board and the motor control unit, a photo-coupler, which allows light to transfer electrical signals between two electrically isolated circuits, is employed between them.

The ESD test for such a myoelectric artificial hand system is expected to the whole system. However, it will be not easy to clarify the reason when a malfunction occurs because there are many factors may cause the malfunction. In view of that the control circuit board is the main part of the system which produces the PWM signals to drive motors, as a first step, we focus the test on the control circuit board. In the first part of this study, we conduct indirect ESD tests on the small size control board (commercially available as REK-0001, Kyoei Sangyo Co. Ltd.) to investigate the basic coupling characteristics of noises induced by an ESD gun. We focus on the influence of ESDs on the pulse width in the PWM signal and an affected pulse width in the PWM output waveforms is defined here as a malfunction of the control board. From a statistical analysis on the pulse width in the PWM signals, we also attempt to clarify the different features in the VCP and HCP cases. In the second part, we examine the effect of photo-coupler in the system because the actual input of the PWM signals to the motor circuit is given through the photo-coupler. We employ the same approach to statistically analyze the pulse width for the photo-coupler's output PWM signals to clarify whether or not it is valid in suppressing the ESD noises. Finally, we also make an attempt to clarify the mechanism based on the experimental findings.

2. Test Method and Conditions

Figures 2(a) and 2(b) shows the test arrangement of indirect discharges from an ESD gun to a VCP and HCP, respectively, for the small size control board. As shown in the figure, the test was conducted according to the IEC 61000-4-2 standard for indirect ESD to a HCP on a table and a VCP on a piece of insulation sheet. The room temperature was 23°C and the relative humidity was 55%. The control board was put on a 1 cm thick styrofoam sheet above the insulation sheet, and at a position of 10 cm far from the VCP. The tip of ESD-gun was set at the center of the HCP or VCP. The control board was powered by a 9 V alkaline battery connected with a 33 cm long power cable between the board and the battery. Such an arrangement was based on the actual usage of the myoelectric artificial hand system, where the battery was usually not located near but at a distance of tens of cm from the control board. So the EUT in this immunity test contained not only the control board but also the power cable and battery.
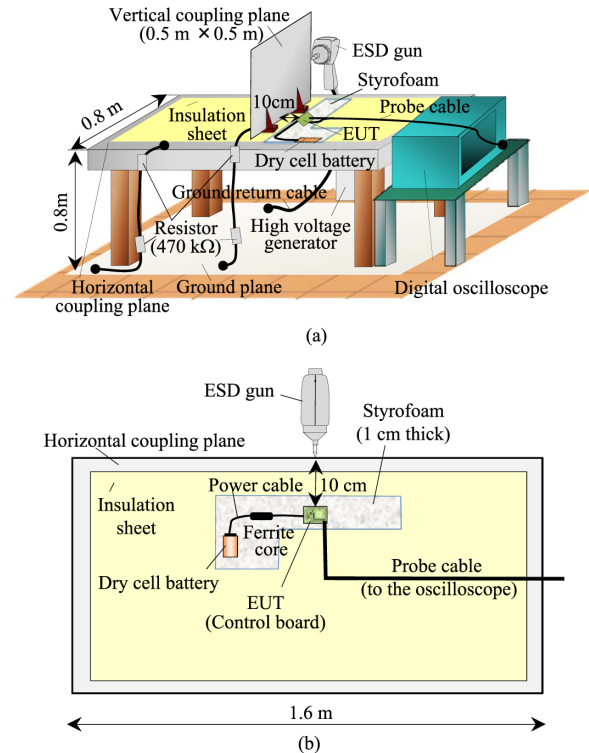

Fig. 2 Test setup for indirect discharges of ESD gun on (a) vertical coupling plane (VCP) and on (b) horizontal coupling plane (HCP).

With this arrangement, a digital oscilloscope (Agilent 54845A, 8 GHz sampling, 1.5 GHz bandwidth) was used to observe the PWM waveforms, and the waveform data were sent to a personal computer by using a USB (Universal Serial Bus) interface in a real-time. Figure 3 shows how the probe of oscilloscope was attached to the PWM signal output pins in the control board. The probe was a 10:1 passive probe with 1 MΩ/12–14 pF input and 500 MHz frequency bandwidth. In order to reduce a direct coupling to the probe cables from the ESD noises, some ferrite cores were attached to the cables.

Figure 4 shows an example of PWM output waveform. The figure is taking voltage on the vertical axis and time on the horizontal axis. The PWM pulse had a magnitude of 5 V, a pulse width of 750 μs and a repetition period of 20 ms. During the ESD test, the disturbance of the pulse width in the PWM output waveforms was analyzed because an affected pulse width may make a malfunction of servo-motors.

Table 1 shows the test conditions. The indirect discharge tests by using the HCP and VCP were conducted under different test levels of ±4 kV and ±8 kV. Under each test level, the test was performed three times. In each test, the ESD events were generated in a burst form. The burst number was 999 times and the time interval between every two events was 50 ms. The PWM waveforms were observed with the digital oscilloscope with a sampling interval of 2 μs. The pulse width for each PWM pulse was extracted from the PWM waveform data using a pre-determined threshold level
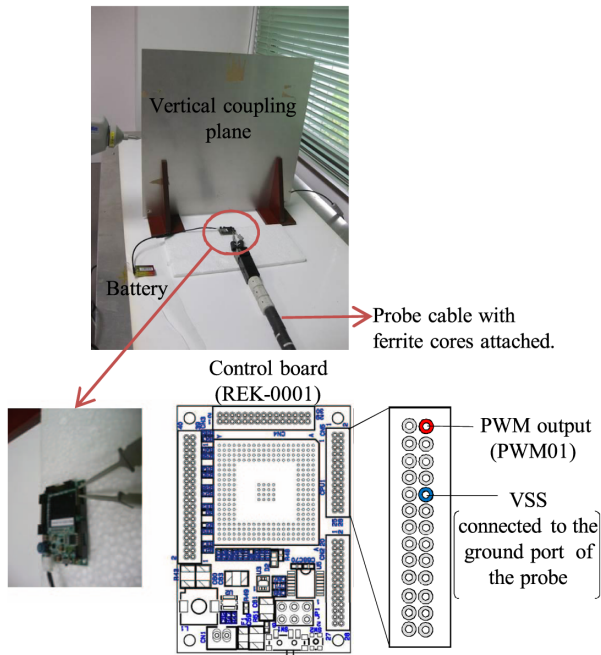
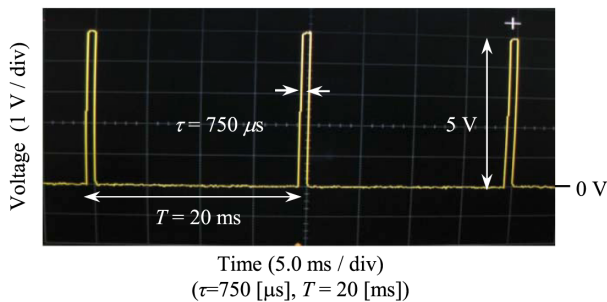**Fig. 3**   Attachment of the probes to acquire the output PWM waveforms.

Fig. 4   Example of PWM time waveform.

Table 1   Specifications of indirect discharge ESD test.

Amplitude of PWM pulse	5 V
Time width of PWM pulse	750 μs
Time period of PWM pulse	20 ms
ESD gun coupling method	VCP and HCP
Test level	4 kV, 8 kV
Porlarity	Positive, Negative
Time interval of burst discharge	50 ms
Number of trial	3
Sampling rate for output to PC	500 kSa/s
Sampling interval for output to PC	2 μs
Pulse detection threshold level	2.5 V

of 2.5 V.

In an actual myoelectric artificial hand system, a photo-coupler is usually used between the control board and a motor control circuit to remove the noises in the PWM signals. To investigate the photo-coupler effect, we observed the PWM waveforms through the photo-coupler connected to a signal output pin of the control board, which will be
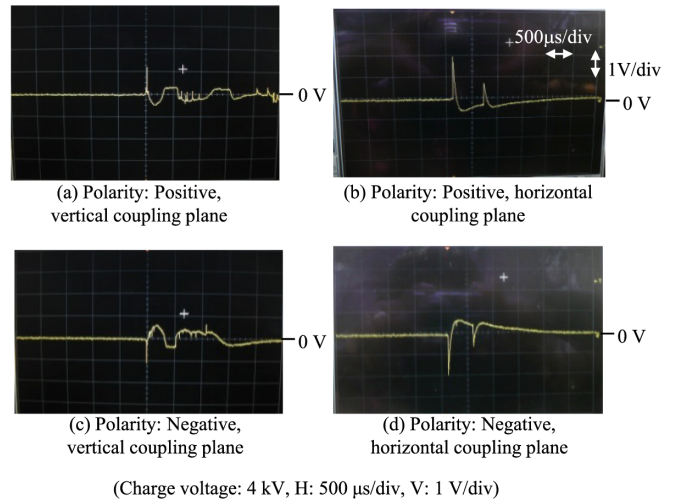

(Charge voltage: 4 kV, H: 500 µs/div, V: 1 V/div)

Fig. 5   Examples of induced ESD noise voltages on power-off PWM output.

discussed in Sect. 4. The test conditions and the analysis method are the same as the case without photo-couplers.

3.   Test Results and Statistical Analysis

Figure 5 shows examples of the voltage waveforms observed at the PMW output pin under the 4 kV test level when the control board was set to power off. The ESD noise voltages exhibit different features for different discharges of polarity, which should yield different effects when they are added to the original PWM signals.

Figure 6 shows two typical examples of ESD noise added to the PWM waveforms under the 8 kV test level. Figure 6(a) shows a type of short time pulses whose pulse width was under the sampling period of 2 µs. In this type the ESD noises did not overlap with the PWM pulses. These pulses are called Type A here. While Fig. 6(b) shows the other type of ESD noises which were superimposed on a PWM pulse. This resulted in that the original PWM pulse with a width of 750 µs was split into two or three parts, and each part of pulses had a width from tens to hundreds µs. These pulses are called Type B. As a result, all of the observed pulses at the PWM output pin can be classified into either Type A or Type B.

Figure 7 shows the percentage of the pulses with different widths (Type A, Type B and PWM) relative to the number of original PWM pulses (in the case without ESD) at the ±4 kV and ±8 kV test levels in the VCP case. It should be noted that their sum is not 100% in total because of the above definition. From the figure, at the ±4 kV test levels, the pulse widths were mainly observed as Type A except for the original PWM pulses. When the test level was ±8 kV, although both Type A and Type B pulses tended to increase, Type A pulses increased more significantly. Moreover, this trend is independent of the polarity of the discharge voltages.

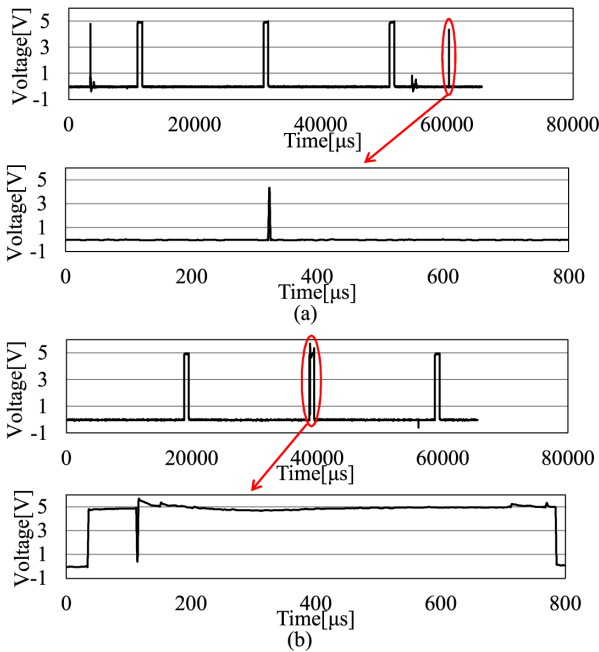Figure 8 shows the relative percentage at the ±4 kV and

Fig. 6 Examples of observed waveforms at the PWM output pin under the 8 kV test level. (a) A type of short time pulses whose pulse width is under the sampling period of $2\,\mu s$; (b) a type of ESD noises which are superimposed on a PWM pulse.
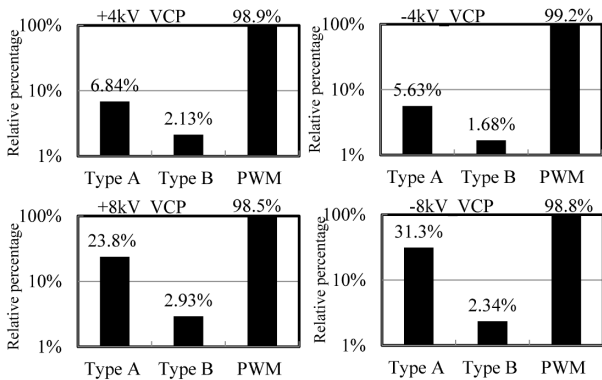

Fig. 7 Relative percentage of various type pulses compared to original PWM pulses in the VCP case.
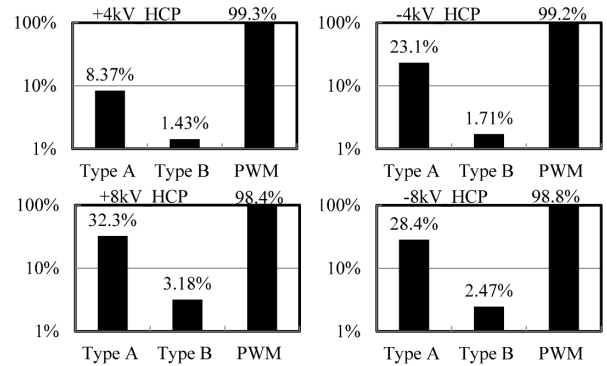

Fig. 8 Relative percentage of various type pulses compared to original PWM pulses in the HCP case.

Fig. 9 Structure of the photo-coupler.

H:10 ms/div
V_{CH1}:1V/div ; V_{CH3}:2V/div

Enlarged view

Fig. 10 Comparison of the PWM input (CH1) and output (CH3) waveforms of the photo-coupler.

±8 kV test levels in the HCP case. Similar to the tests in the VCP case, the observed pulses mainly belong to Type A, and there is an obvious increase at −4 kV/m in the HCP case compared to the VCP case. Under most test conditions, the Type A and Type B noises in the HCP case were found to take a larger percentage than that in the VCP case. In view of that the EUT is located right above the HCP, the ESD interference in the HCP case should be stronger than the VCP case.

4. Noise Suppression Effect of Photo-Coupler

As in the actual artificial hand system, a photo-coupler (Toshiba TLP281, Rising/falling time: 2–$3\,\mu s$) as shown in

Fig. 9 was connected to a PWM signal pin of the control board with a very short cable (2 cm). The ESD suppression effect of the photo-coupler was therefore investigated as follows.

4.1 Test Results

At first, the input (CH1) and output (CH3) PWM waveforms of the photo-coupler were observed, and the waveform data were sent to the computer for further analysis. Figure 10 shows two typical PWM waveforms before and

Fig. 11 Relative percentage of various type pulses compared to original PWM pulses in the VCP case for comparison of photo-coupler effect.
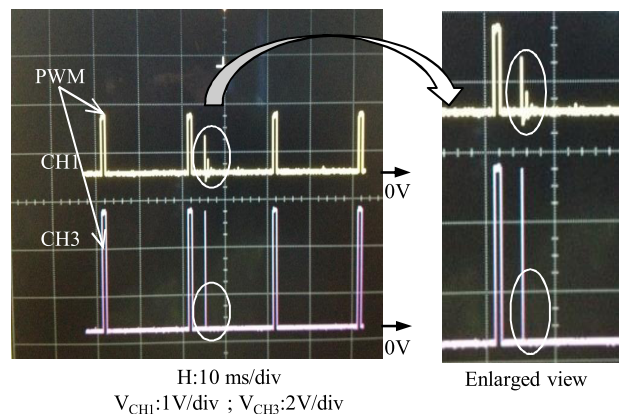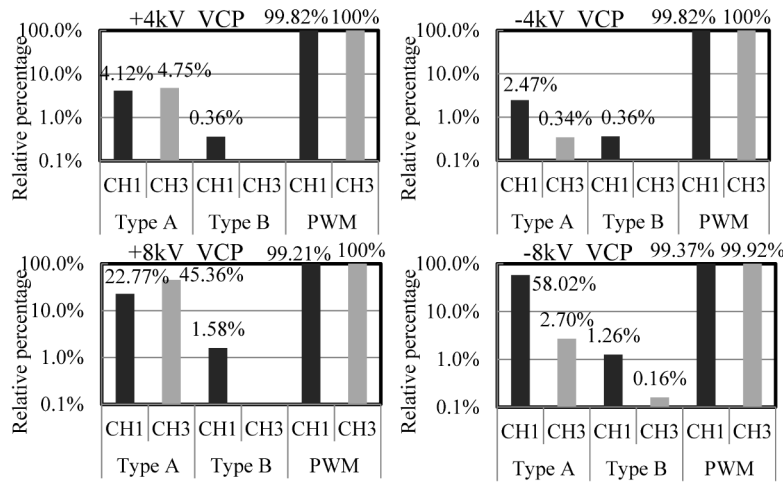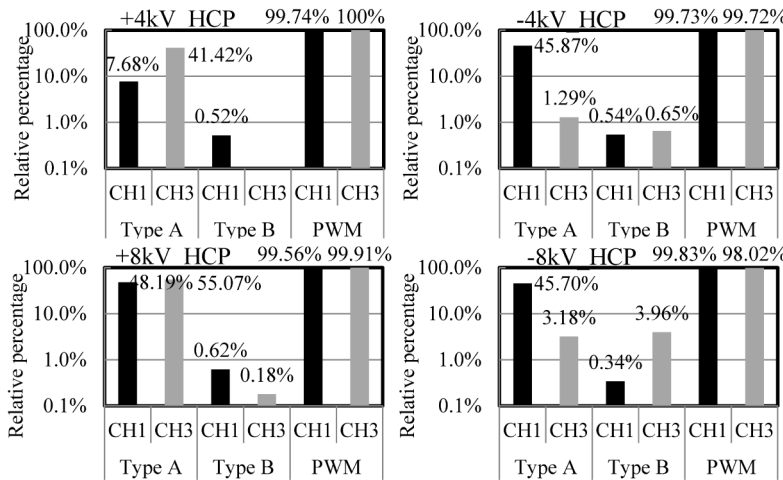

Fig. 12 Relative percentage of various type pulses compared to original PWM pulses in the HCP case for comparison of photo-coupler effect.

after the photo-coupler under the 4 kV ESD test level in the VCP case. By comparing the input and output waveforms of the photo-coupler in the figure, we could see that, except for the first ESD noise peak, the next ESD pulses with smaller magnitude were removed after the photo-coupler. This phenomenon may be considered as the following two reasons. First, the smaller noises had not a voltage or current large enough to drive the transistor in the output side of the photo-coupler, which yielded that they did not appear at the output side of the photo-coupler. Second, due to the presence of parasitic capacitance between the input and output of the photo-coupler, only the low-frequency components were filtered by the photo-coupler, whereas the high-frequency components passed through the photo-coupler or the parasitic capacitance.

Figures 11 and 12 show that, compared to the original PWM pulse number without the ESD, how many pulses take different pulse widths when the PWM signals pass through

the photo-coupler under the ESD test. As can be seen, Type A pulses become more dominant for the positive polarity but less dominant for the negative polarity after the signals get through the photo-coupler, while Type B pulses become less dominant except for the negative polarity in the HCP case. It may be explained by that the ESD noises with the magnitude smaller than the 2.5 V threshold may be pulled up to nearly 5 V after the signals get through the photo-coupler for Type A pulse noises, as long as they have a sufficient magnitude to drive the photo-coupler. The Type B pulse noises resulted from an addition of ESD noises to the original PWM signals as show in Fig. 6(b). Since the rising/falling time of the pulses is slowed down slightly after the photo-couple, the narrow pulse noises, that divide the original PWM signal into two or three parts, may be smoothed so that the number of Type B pulse noises decrease. In the HCP case for negative polarity, however, the original PWM signals are easier to be divided into two or three parts with deeper dips
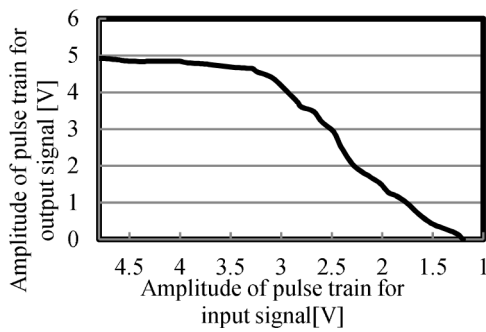
Fig. 13 Relationship between the amplitudes of input and output voltage of the photo-coupler.

Fig. 14 Experimental circuit to measure the frequency feature of the photo-coupler.

Fig. 15 Relationship between the frequency of input signal and the amplitude of output voltage of photo-coupler from 1 MHz to 3 GHz, which covers the possible frequency range of ESD noise as shown in [6].

because of the large noise level of negative polarity. The above-mentioned rising/falling time is not long enough to smooth them, so an increase in Type B is observed.

4.2 Discussion

For clarifying the mechanism of the photo-coupler in ESD noise suppression, we conducted an extra experiment which focused on the relationship of the driving capability between the input and output signals of the photo-coupler. Referring to Fig. 9, since the signal is transmitted through light inside the photo-coupler and we could only know the electric signal, we used a signal generator to control the input voltage and then the current.

Figure 13 shows the relationship between the amplitudes of input and output of a PWM signal with a constant period (20 ms) and pulse width (750 μs). As can be seen, as the input PWM signal amplitude decreases to about 1.2 V, the output voltage of the photo-coupler becomes zero. In other words, if the noise voltage is less than 1.2 V, the photo-coupler will not be driven and the corresponding noise can be removed. However, when the noise voltage is larger than 1.2 V, it may pass through the photo-coupler and be pulled up to 5 V to exceed the threshold of 2.5 V. This mechanism should yield the increase of Type A pulse noises after the photo-coupler.

In addition, the presence of parasitic capacitance between the input and output of the photo-coupler may also yield a capacitive coupling and then reduce the suppression effect on high-frequency ESD noises. So we conducted another experiment whose circuit is shown in Fig. 14. In this experiment, we set the amplitude of the source voltage (V_s) to 1 V and the internal resistance (R_s) to 50 Ω for the signal generator, which is not large enough to drive the transistor inside the photo-coupler. Since the ESD noise may have a frequency range up to several GHz, as shown in [6], for example, we measured the relationship between the frequency of input signal and the amplitude of output voltage of the photo-coupler from 1 MHz to 3 GHz. As can be seen in Fig. 15, even a small input signal could still get through the photo-coupler at higher frequencies. From the point of intersection of the tangent line of the rising part and the steady
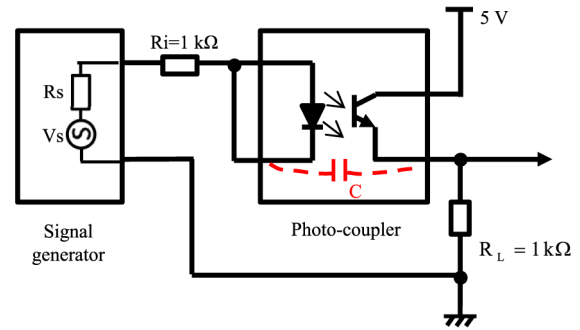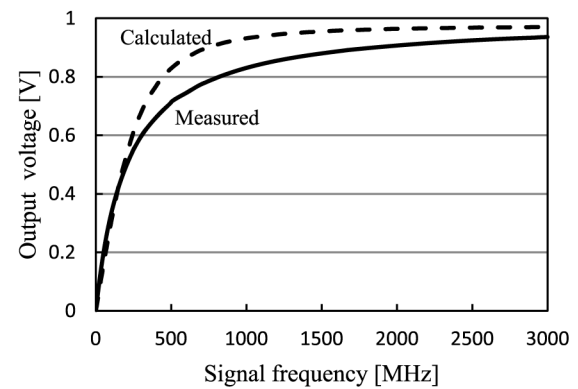
state voltage in Fig. 15, we could derived the corresponding frequency f_c as 300 MHz approximately, and then the parasitic capacitance of 0.25 pF from $C = 1/2\pi f_c (R_s + R_i + R_L)$ where R_i and R_L are shown in Fig. 14. Using this estimated parasitic capacitance C, we calculated the output voltage from

$$V_o = \frac{4\pi f C R_L}{1 + [2\pi f C (R_s + R_i + R_L)]^2} V_s \tag{1}$$

for $V_s = 1$ V and also plotted the result in Fig. 15 with a dashed line. The reasonable agreement between them supports the explanation of the capacitive coupling between the input and output of the photo-coupler at high frequencies.

In reality, the above-mentioned two mechanisms should work together to affect the noise suppression effect of the photo-coupler.

5. Conclusions

An indirect ESD immunity test has been conducted, in accordance with IEC 61000-4-2, on a small control board used in a myoelectric artificial hand system. The PWM pulses are sent from the control board to a motor control circuit, and a photo-coupler is used between them for suppressing noises.

First, at the PWM signal output pins, two types of

pulses, different from the original PWM pulse, have been observed. One type is due to the ESD noise itself, and the other type is due to a superimposition of the ESD noise to the PWM pulses. Both types of pulses can be observed regardless of the charge voltages of the ESD gun, and Type A dominates the noise pulses. Moreover, the ESD interference is stronger in the HCP case than that in the VCP case. The findings have demonstrated the basic characteristics of the indirect ESD impact on the PWM pulses in the small size control board.

Second, the test results for the ESD noise suppression effect of a photo-coupler also confirm the findings mentioned above. Moreover, it is found that Type A noises tend to increase for positive polarity and decrease for negative polarity after the photo-coupler, and Type B noises also tend to increase for negative polarity in the HCP case. The findings suggest that the photo-coupler can not function well as expected in ESD suppression. One of the reasons has been demonstrated to be due to the driving capability of the photo-coupler, and the other one is due to the presence of parasitic capacitance between the input and output of the photo-coupler. Such capacitive coupling reduces the suppression effect on high-frequency ESD noises.

The future subject is to further clarify the ESD coupling route and then derive an effective ESD countermeasure.

Acknowledgments

References

[1] Japanese Industrial Standards Committee, "Electromagnetic compatibility (EMC) — Part4: Testing and measurement techniques — Sect. 2. Electrostatic discharge immunity test," JIS C 61000-4-2 (IEC 61000-4-2: 1995/Amd.1), 1999 (in Japanese).

[2] IEC (International Electrotechnical Commission), "IEC 61000: Electromagnetic compatibility (EMC) Part 4: Testing and measurement techniques, Sect. 2: Electrostatic discharge immunity test," Edition 2.0, Dec. 2008.

[3] J. Koo, Q. Cai, K. Wang, J. Maas, T. Takahashi, A. Martwick, and D. Pommerenke, "Correlation between EUT failure levels and ESD generator parameters," IEEE Trans. Electromagn. Compat., vol.50, no.4, pp.794–801, Nov. 2008.

[4] J. Baran and J. Sroka, "Uncertainty of ESD pulse metrics due to dynamic properties of oscilloscope," IEEE Trans. Electromagn. Compat., vol.50, no.4, pp.802–809, Nov. 2008.

[5] T. Taka and O. Fujiwarea, "Variations in discharge current waveforms and its power spectra injected from contact discharges of ESD-gun with different arrangements," IEEJ Trans. Fundament. & Materials, vol.131, no.3, pp.384–388, May 2011 (in Japanese).

[6] J. Baran and J. Sroka, "Frequency approach to analysis of ESD pulse," IEEJ Trans. Fundament. & Materials, vol.132, no.5, pp.339–344, May 2012.

[7] F. Toya, I. Mori, O. Fujiwara, Y. Taka, S. Ishigami and Y. Yamanaka, "Estimation of discharge currents for contact discharges from ESD gun to equipment under test," IEICE Trans. Electron. (Japanese Edition), vol.J94-C, pp.288–295, Oct. 2011.

[8] N. Yamamoto, Y. Taka, and O. Fujiwara, "Uncertainty and its reduction of voltage waveform induced on trace on printed circuit board for indirect discharges from ESD-gun onto vertical coupling plane," IEEJ Trans. Fundament. & Materials, vol.130, no.3, pp.253–257, March 2010 (in Japanese).

[9] N. Yamamoto, Y. Taka, and O. Fujiwara, "A new method for immunity testing less dependent on arrangements of equipment-under-test and contact discharges of ESD-gun onto vertical coupling plane," IEEJ Trans. Fundament. & Materials, vol.130, no.5, pp.423–427, May 2010 (in Japanese).

[10] T. Tsuji, Y. Taka, O. Fujiwara, and N. Yamamoto, "Variations in electromagnetic fields spatially induced for indirect discharges of ESD-gun of ESD generators onto vertical coupling plane," IEEJ Trans. Fundament. & Materials, vol.131, no.2, pp.119–124, Feb. 2011 (in Japanese).

[11] T. Tsuji, K. Himeno, and O. Fujiwara, "Reduction of variation in magnetic fields and its experimental verification for indirect discharges of ESD generators onto tapered-type vertical coupling plane," IEEJ Trans. Fundament.& Materials, vol.132, no.1, pp.51–56, Jan. 2012 (in Japanese).

Cheng Ji received the B.E. degree from Nanjing University of Posts and Telecommunications, Nanjing, China, in 2010, and the M.E. degree from Nagoya Institute of Technology, Nagoya, Japan, in 2015, where he was involved in the research on ESD immunity tests.

Daisuke Anzai received the B.E., M.E. and Ph.D. degrees from Osaka City University, Osaka, Japan in 2006, 2008 and 2011, respectively. Since April 2011, he has been an Assistant Professor at the Graduate School of Engineering, Nagoya Institute of Technology, Nagoya, Japan. He has been engaged in the research of biomedical communication systems and localization systems in wireless communication networks.

Jianqing Wang received the B.E. degree in electronic engineering from Beijing Institute of Technology, Beijing, China, in 1984, and the M.E. and D.E. degrees in electrical and communication engineering from Tohoku University, Sendai, Japan, in 1988 and 1991, respectively. He was a Research Associate at Tohoku University and a Senior Engineer at Sopia Systems Co.,Ltd., prior to joining the Nagoya Institute of Technology, Nagoya, Japan, in 1997, where he is currently a Professor. His research interests include biomedical communications and electromagnetic compatibility.

Ikuko Mori received the B.E. and M.E. degrees in electrical and information engineering and the D.E. degree in information Engineering from Nagoya Institute of Technology, Nagoya, Japan, in 2002, 2004 and 2007, respectively. She has joined Department of Electronic and Information Engineering, Suzuka National College of Technology, Suzuka, Japan since April 2007, where she is currently an Assistant Professor. Her research interests include ElectroStatic Discharge (ESD) and Electromagnetic Compatibility related ESDs.

Osamu Fujiwara received the B.E. degree in electronic engineering from the Nagoya Institute of Technology, Nagoya, Japan, in 1971, and the M.E. and D.E. degrees from Nagoya University, Nagoya, Japan, in 1973 and 1980, respectively, both in electrical engineering. From 1973 to 1976, he was with the Central Research Laboratory, Hitachi Ltd., Kokubunji, Japan, where he was engaged in research and development of system packaging designs for computers. From 1980 to 1984, he was with the Department of Electrical Engineering, Nagoya University, as a Research Associate, and from 1984 to 1985, as an Assistant Professor. In 1985, he joined the Nagoya Institute of Technology, as an Associate Professor. In 1993, he became a Professor with the Graduate School of Engineering, Nagoya Institute of Technology. In 2012, he retired and became an Emeritus Professor with the Nagoya Institute of Technology. His research interests include measurement and control of EM interference due to discharge, bioelectromagnetics, and other related areas of EM compatibility.